Concertina effect-based underwater structure inspection by autonomous vehicles in three dimensions

Concertina Effect-based Underwater Structure Inspection by Autonomous Vehicles in Three Dimensions

David McIntyre
School of Electronics, Electrical Engineering and Computer Science
Queen's University Belfast
Email: dmcintyre04@qub.ac.uk

Wasif Naeem
School of Electronics, Electrical Engineering and Computer Science
Queen's University Belfast
Email: w.naeem@qub.ac.uk

Syed Saad Azhar Ali
Center for Intelligent Signal & Imaging Research,
Universiti Teknologi PETRONAS,
32610 Seri Iskandar, Perak, Malaysia
Email: saad.azhar@utp.edu.my

***Abstract*—Autonomous underwater vehicles (AUVs) are becoming increasingly widespread in today's industrialised world, with research shifting towards cooperative control between multiple vehicles. Cooperative control between AUVs poses a number of challenges such as collision-avoidance, path-planning and group formation. This paper presents a novel 3D technique for the purposes of inspecting underwater structures using autonomous vehicles. Vehicles are navigated using a combination of traditional artificial potential fields (APFs) and rotational potential fields (RPFs) which are employed using 2D sub-planes in a concertina effect to provide full boundary coverage and inspection of submerged architectures. Vehicles are freed from the usual angular constraints associated with group strategies whilst moving in a fluid formation, reducing computational load. Simulation results show the effectiveness of the technique on two different-sized structures, providing varying customised levels of inspection and successful collision-free journeys throughout with minimal path length.**

***Keywords* - autonomous underwater vehicles (AUVs), artificial potential fields (APFs), rotational potential fields (RPFs), cooperative control, underwater inspection, mapping and surveying**

I. Introduction

In today's society autonomous vehicles are becoming increasingly commonplace with rapid developments in computing power opening up many exciting avenues in the field of robotics. News items on autonomous road vehicles and airborne drones regularly portray their amalgamation into everyday life. Yet despite these advancements, the underwater world, rich in biodiversity and a vast expanse of unexplored structures, remains under-utilised. From this perspective, the scope for underwater vehicle use remains almost boundless.

The first real developments in the field of AUVs began in the 1980s following the increase of low-powered computers coupled with improved software capabilities. Research funding increased during the 1990s, and the advent of the 21st century heralded a new age of underwater exploration, when the commercial market began to grow. AUVs range from huge, multi-million dollar behemoths weighing over 60 tonnes (used for large scale industrial projects) [1], right down to small hand-held models designed for hobbyists with a price tag of just a few hundred dollars [2]. Uses are widespread, covering different fields of interest, for example, scientific applications include water quality testing, data-gathering, offshore mapping, marine biology inspection etc. [3], industrial and commercial applications (dominated by the oil and gas industry [4]) include the inspection of underwater structures such as oil rigs and pipelines [5], and the military use them for intelligence-gathering, communications, navigation and eradicating underwater mines [6] to name a few. Recently there has been an increase in popularity for small, inexpensive models, and concerns are being raised as to the impact on the underwater environment [7].

Over the past number of years, the great need for multiple AUVs (MAUVs) working together within a cooperative framework has been highlighted following crises such as the BP oil spill disaster in 2010 [8] and the tragic disappearance (and subsequently, so far unsuccessful search) of Malaysia Airlines flight MH370 in 2014 [9]. MAUVs are now a very viable prospect given today's technology, along with developments in communications, and research is growing in this area. Alongside exploration and crisis management a great number of man-made underwater structures exist requiring regular inspection. Currently hundreds of offshore rigs are dotted around the planet, dedicated to the acquisition of fossil fuels such as oil and natural gas, with at least 184 in the North Sea alone [10]. It should be expected that the recent drive towards clean and renewable energy sources would reduce the number of rigs offshore, however, due to the size and aesthetics of turbines, wind-farms are now being placed in the sea in an effort to preserve the countryside. The United Kingdom currently leads the world in per capita generation, producing 5% of its annual electricity requirements from at least 20 offshore farms, a percentage expected to double by 2020 [11]. Given that the cost of a single turbine can be in excess of £3.25 million [12], it is imperative to perform regular inspections, ensuring continued efficiency whilst reducing long-term costs.

In parallel with industrial expansion, grand ideas are currently in development to ease the burden of over-population in certain regions of the world by constructing large floating cities. Studies

are ongoing to produce these permanent communities off the coasts of existing nations, providing unique living environments in close proximity to land borders [13]. Combining this with the vast number of piers, jetties and wharfs across the globe, alongside natural underwater structures, one can see that the need for MAUV groups will increase significantly in line with both industrial and social development.

The cooperative control framework around multiple vehicles contains a number of prominent challenges including collision avoidance (both intra and inter-vehicle), localisation and communications. As a vehicle's depth increases it is forced to rely on dead-reckoning techniques (or periodic resurfacing) to keep an accurate track of its position, as the water's surface acts as a barrier to GPS. Underwater communication is limited and severely attenuated by salinity levels and low bandwidth, these, coupled with multi-path echoing pose challenges to real-time reception [14]. Power and energy consumption during long-term missions, alongside operation within the confines of a dynamic and uncertain environment, can lead to vehicle failure or loss. Collision avoidance is also a major area, and essential for improved autonomy and mission success. Challenges within this field include inter-vehicle collisions within group formations alongside both static and dynamic obstacles. Path-planning and guidance are additional spheres within which solid design consideration is a necessity. Thus, to enable true cooperation between platforms, proper design of control architecture is essential.

II. Background and Overview

To overcome the challenges listed above, a number of techniques and control architectures have been developed in recent years. These can be broadly classified into two main categories - centralised and decentralised. In the *centralised* architecture, each vehicle is linked to a central controller and periodically receives information pertaining to the current mission, whereas in the *decentralised* architecture, independent agents generally act alone, whilst maintaining communication links to some or all of the other agents. The two categories are not mutually exclusive and may include aspects of either area, depending on a range of factors such as fleet size, sensor range and mission objectives to name a few. The above techniques are further classified into three broad fields - behaviour-based, leader-follower and virtual structures (falling into both centralised and decentralised domains and/or a mix of the two).

Behaviour-based: inspired by the animal world, vehicles operating under this model generally perform sense-and-react manoeuvring. Behavioural rules vary dramatically in both scope and speed and depend upon a range of variables linked to mission objectives, working environment, vehicle capabilities etc. Rule prioritisation is often organised by the assignment of iterative cost functions. One successful application of the behaviour-based strategy has been made in the modelling of fish schooling behaviour [15].

Leader-follower: a single vehicle (or vehicles), programmed with path-planning or guidance capabilities leads a group of follower agents towards a point of interest. Cost reduction can be considerable as followers are generally only concerned with their position relative to the leader, requiring less complex hardware. A leader vehicle may transmit concurrent coordinates to each follower or remain independent, and certain followers can be suitably equipped to replace leader vehicles for system robustness in the case of leader failure [16].

Virtual Structures: MAUVs often group into a rigid formation or shape which then moves in its entirety through an environment towards a goal position. An imaginary vehicle may be employed for this technique, placed at a strategic position within the group, enabling all others to maintain a specified distance and angle from it to preserve the formation [17].

A. Artificial Potential Fields

In the 1980s, research by O. Khatib guided a vehicle to an intended goal, whilst avoiding obstacles, using the analogy of a potential field. A combination of repulsive fields surrounding obstacles, coupled with an attraction at the intended goal position (creating an overall field), was used to guide the agent [18].

An attractive field towards the goal position was created using Equation 1

$$Ux_d(x) = \frac{1}{2}k(x - x_d)^2 \tag{1}$$

where $Ux_d(x)$ is the attractive potential field from the goal, x is the current position of the agent, x_d is desired goal and k is a scaling factor.

To ensure a collision-free journey, repulsive fields were formed around obstacles to prevent collisions using Equation 2.

$$U_o(x) = \begin{cases} \frac{1}{2}\eta(\frac{1}{\rho} - \frac{1}{\rho_o})^2 & \text{if } \rho \leq \rho_o \\ 0 & \text{if } \rho \geq \rho_o \end{cases} \tag{2}$$

where $U_o(x)$ is the repulsive force around each obstacle, ρ_o is the limit distance of the potential field, ρ is the shortest distance from vehicle to obstacle O whilst η is a scaling factor.

The popularity and use of APFs has fluctuated over the decades but, being computationally inexpensive, they have been used in a number of different areas and also enhanced to include multiple vehicles [19]. A limited number of papers have extended their use into three-dimensional work for both airborne [20], and underwater vehicles [21]. A frequently reported issue with this method is when attractive and repulsive forces combine to produce a null force, leading the vehicle to become trapped in a local minimum and remain in a static position. A further issue prevents a goal position being reached due to a near-by obstacle and is commonly known as the GNRON problem (goal nonreachable by obstacles nearby). Various solutions to solve these problems have been proposed, such as simulated annealing [22] or the creation of a nearby virtual object [**?**].

B. Rotational Potential Fields

Rotational potential fields (RPFs), a variant of APFs, have also been employed to solve the local minima problem by driving vehicles around obstacles in a circular manner. Clockwise or anticlockwise fields are created using tangential vectors in place of direct repulsion (see Fig 1), the force of which increases as vehicle distance-to-obstacle decreases.

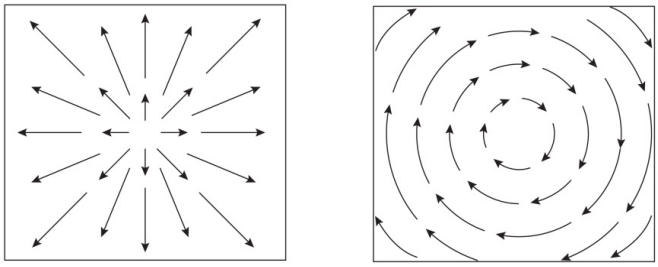

Fig. 1: Original Potential Fields vs Rotational Potential Fields [23]

RPFs, by their very nature, work most efficiently within a two dimensional plane, and research has mainly been focused in this area. For example, in [24] a single ground-based, wheeled robot is guided towards a goal within a 2D environment, while RPFs guide it around obstacles on a nearest-edge basis. Work involving multiple vehicles also tends to focus on the guidance of rigid vehicle structures. For instance, in [25] the entire vehicle formation is guided towards a goal without splitting (on a 2D plane), using RPFs for obstacle avoidance. In [26], use is made of a virtual vehicle to guide a rigid 2D group of vehicles to an intended target, which meets an obstacle head on before splitting and recombining. Extending the technique into three dimensions, in [27] a single unmanned aircraft uses rotational fields to avoid obstacles, again on a nearest-edge basis.

This paper presents a novel technique allowing rotational fields to be employed within a three dimensional environment for the purposes of inspecting the supporting columns of an off-shore oil platform. A pair of vehicles are guided by traditional APFs in a fluid formation before surveying each column in turn using a concertina effect, where both vehicles switch between an $\mathbb{R}^2$ subplane within $\mathbb{R}^3$, allowing guidance by opposing RPFs. Rotational fields significantly reduce the issue of local minima and adjustable waypoints (to increase or decrease the diameter of the circular field) tackle the GNRON problem. In addition, a rigid structure is dispensed with in favour of a fluid formation (where vehicle separation is the only inter-dependent constraint), eliminating the need for a virtual vehicle thus reducing overall computational load. Vehicles will employ both attractive and repulsive fields to maintain a pre-determined separation without angular constraints. Every column is surveyed to a user-definable level of accuracy, with path minimisation prioritised to conserve power and reduce costs. The technique can be utilised for different sized structures at varying depths.

The remainder of the paper is organised as follows. Section III explains the foundational work including object survey by a fluid vehicle formation using opposing RPFs within a three dimensional environment. Section IV details the proposed methodology, covering column inspection order, waypoint placement, user-adjustable survey parameters and forming suitable $\mathbb{R}^2$ sub-planes. Section V displays simulated results on two different sized structures using varying defined inspection parameters. Section VI covers analysis of the simulation results with the conclusion following in Section VII.

III. Mathematical Theory

While research involving RPFs in three dimensions is limited, it has been previously shown by the authors that opposing rotational fields can be employed by a pair of vehicles for object survey within a three dimensional environment [**?**]. For convenience the main findings in [**?**] will form the rest of this section along with a relevant selection of the results as it forms an integral component of this new technique (for a full account of the method including waypoint placement and numerical results etc. please refer directly to the paper).

A. Object Survey in $\mathbb{R}^3$ using Opposing Rotational Fields

A pair of vehicles are guided by traditional APFs towards each object of interest in turn. As vehicles approach the object boundary they are split and utilise rotational fields, which guide them around opposing sides for survey purposes.

Traditional Fields: Potential fields work using a gradient descent method i.e. an attractive pole acts in a similar manner to an energy well, driving vehicles towards its lowest point. Repulsive fields can be imagined as 'rounded hills' protruding from this energy well, for the purpose of obstacle avoidance. At each coordinate within the working environment, the negative gradient can be determined and there are many variations on the original equations. Attractive and repulsive vectors are then summed at each point to produce an overall force vector. Attractive goals or waypoints can be described by using the gradient equation (3)

$$\mathbf{F}^{att}_{w_i}(\mathbf{x}) = -\nabla U^{att}_{w_i}(\mathbf{x}) = k_a(\mathbf{x} - \mathbf{x}_{w_i}) \tag{3}$$

where $\mathbf{F}^{att}_{w_i}(\mathbf{x})$ is the attractive force vector due to waypoint i acting on the coordinates $\mathbf{x}$ in a three-dimensional Euclidean space $\mathbb{R}^3$ (herein after referred to as a *point* or *position*), $-\nabla U^{att}_{w_i}(\mathbf{x})$ is the negative gradient due to the attractive force of waypoint i at the point $\mathbf{x}$, k_a is a force scaling factor and $\mathbf{x}_{w_i}$ is the position of waypoint i.

Repulsion, radiating isotropically from a point, can be described by (4), where the force is a factor of the squared distance between the vehicle and repulsive centre.

$$\mathbf{F}^{rep}_{o_i}(\mathbf{x}) = -\nabla U^{rep}_{o_i}(\mathbf{x}) = k_r(\mathbf{x} - \mathbf{x}_{o_i})d^{-3/2} \tag{4}$$

where $\mathbf{F}^{rep}_{o_i}(\mathbf{x})$ is the repulsive force vector due to object i acting at the point $\mathbf{x}$, $-\nabla U^{rep}_{o_i}(\mathbf{x})$ is the negative gradient due to the repulsive force of object i at the point $\mathbf{x}$, k_r is a

force scaling factor, $\mathbf{x}_{o_i}$ is the position of object i and d is the shortest distance between the vehicle and object.

A number of points are used within $\mathbb{R}^3$ to approximate the shape of an object's surface. Each of these acts as a point-source repulsion in its own right, and the combined sum of vector forces serves as an overall repulsion at each coordinate within $\mathbb{R}^3$. However, it should be noted that this combined force is only employed within a distance threshold of the object surface, and is described by (5)

$$\mathbf{F}^{rep}_{o_{res}}(\mathbf{x}) = -\nabla U^{rep}_{o_{res}}(\mathbf{x}) = \begin{cases} \sum_{p_o=1}^{p_o=m} k_r(\mathbf{x}_{N_i} - \mathbf{x}_{o_i}) d_{p_o}^{-3/2} & \text{if } d_{p_o} \leq r_{o_i} \\ 0 & \text{if } d_{p_o} > r_{o_i} \end{cases} \quad (5)$$

where $\mathbf{F}^{rep}_{o_{res}}(\mathbf{x})$ is the overall resultant force vector acting on a point $\mathbf{x}$ due to the sum of every repulsive vector emanating from a set of m points on the surface of an object O, $-\nabla U^{rep}_{o_{res}}(\mathbf{x})$ represents the negative gradient due to this resultant force, k_r is a force scaling factor, $\mathbf{x}_{N_i}$ is the position of vehicle $i \in N$ (where N is the set of vehicles), $\mathbf{x}_{o_i}$ is a point on the surface of the object, d_{p_o} is the distance from the vehicle to the current object surface point and r_{o_i} is the range of influence of object repulsion.

Rotational Fields: In order to achieve clockwise and anti-clockwise fields around each object, tangential force vectors were formed on the $x-y$, $\mathbb{R}^2$ plane. To accomplish this, each resultant force vector radiating isotropically from an object ($\mathbf{F}^{rep}_{o_{res}}$ - determined from Equation 5), is broken down into its x, y & z component vectors. As opposing rotational fields are only achieved on a 2D plane, the z component is removed, leaving the x & y vectors. These two vectors are then either summed or subtracted in order to create the rotational fields around the object.

B. Fluid Formation

A novel approach was used which dispensed with the need for a rigid structure and/or a virtual vehicle. The lack of need for angular constraint produces a more fluid flow, yet ensures vehicles maintain an approximate separation distance when not in surveying mode. Depending on the distance between v_1 & v_2, APF Equations 3 & 4 are used to assign either an attractive or repulsive force to v_2, which then acts upon v_1 depending on the desired separation, s_v, set by the user.

C. Object Survey

As the vehicle pair approaches each object, v_1 & v_2 must each be assigned an opposing rotational field to ensure that the entire item of interest is encircled. In the case of each vehicle pair, three vectors as depicted in Fig 2 are used to determine which field is assigned to each vehicle during a survey, 1) $\overrightarrow{o_i w_i}$ from object centre to the current waypoint, 2) $\overrightarrow{o_i v_1}$ from object centre to vehicle 1, and 3) $\overrightarrow{o_i v_2}$ from object centre to vehicle 2. In Fig 2, angles α & θ are measured in a clockwise direction from $\overrightarrow{o_i v_2}$ & $\overrightarrow{o_i v_1}$ to $\overrightarrow{o_i w_i}$ respectively and compared in magnitude. The vehicle with the largest angle is then assigned an anticlockwise direction around the object. In every instance both vehicles are allocated opposing fields, regardless of their direction of travel (in the rare case where vehicles approach using the same angle, each is arbitrarily assigned its own field of rotation).

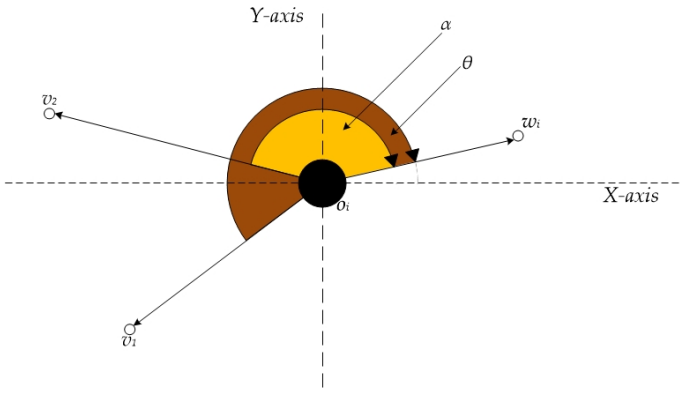

Fig. 2: Calculation of angle for assignment of rotational fields (Note: vectors shown are for the purposes of field assignment and do not denote direction of vehicle travel)

D. Translating Between $\mathbb{R}^3$ and $\mathbb{R}^2$

The use of rotational fields in the $x-y$ plane disrupts the smooth trajectory of a vehicle within $\mathbb{R}^3$, as seen in Fig 3.

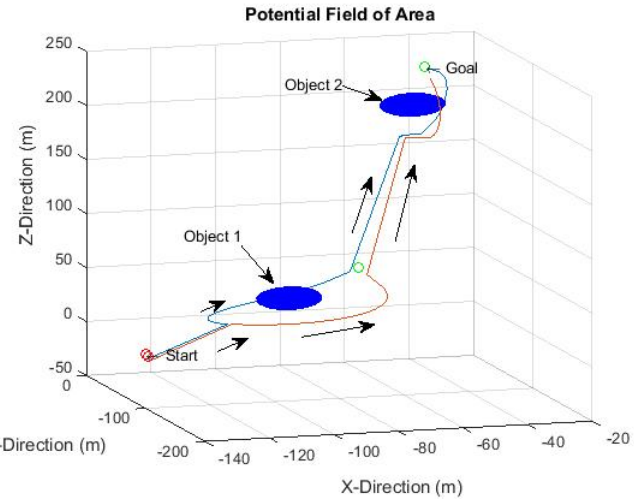

Fig. 3: Example of $x-y$ rotational fields within $\mathbb{R}^3$

Fig 3 above shows a vehicle pair encircling two objects before arriving at a goal position. In the case of object 1, a near-horizontal approach shows a relatively smooth trajectory around the object's boundary. The approach towards object 2, however, takes a much steeper angle: it can be seen that the trajectory of both vehicles around the object is impaired by the horizontal repulsion. The technique therefore created a unique local 2D plane around each object within which a smooth rotation can be achieved. The local 2D plane in question is determined when both vehicles enter the range of influence of the rotational fields, and it lies on the points connecting the

object centre with v_1 & v_2. Creating a two dimensional plane within a 3D environment, whereby coordinates can be easily interchanged between the two, involves a number of steps. To illustrate this, the case of two vehicles (v_1 & v_2) and an object (O_i) within $\mathbb{R}^3$ will be used. The 2D plane will be formed such that v_1, v_2 and O_i all lie upon it simultaneously.

The steps involve creating a transformation matrix, enabling coordinates to be converted from $\mathbb{R}^3$ (the global reference frame) onto the $\mathbb{R}^2$ plane (local reference frame). Let both vehicles have coordinates $v_1 = (v_{1_x}, v_{1_y}, v_{1_z})$ & $v_2 = (v_{2_x}, v_{2_y}, v_{2_z})$ and object $O_i = (O_{i_x}, O_{i_y}, O_{i_z})$.

1) Creating Local Reference Frame: Step 1: move object to the centre of the new origin i.e.
$O'_i = (0 - O_{i_x}, 0 - O_{i_y}, 0 - O_{i_z}) = (-O_{i_x}, -O_{i_y}, -O_{i_z})$

Step 2: apply the same shift to v_1 & v_2 i.e. $v'_1 = (v_{1_x} - O_{i_x}, v_{1_y} - O_{i_y}, v_{1_z} - O_{i_z})$ & $v'_2 = (v_{2_x} - O_{i_x}, v_{2_y} - O_{i_y}, v_{2_z} - O_{i_z})$

To successfully translate between reference frames, three new axes within the local environment are required to represent the translated x, y & z coordinates. These are assigned by the formation of three unit vectors (using both vehicle and objects from the global frame) as in Step 3 below.

Step 3: the first unit vector is formed by the normalisation of the vector between O_i and v_1, and acts as the x-axis of the new local frame.

$$\hat{\mathbf{t}} = \frac{(v'_1 - O'_i)}{|(v'_1 - O'_i)|} \tag{6}$$

Step 4: taking the normalisation of the cross product of $\hat{\mathbf{t}}$ and the vector between O_i & v_2 gives a vector orthogonal to $\hat{\mathbf{t}}$ which acts as the y-axis of the new local frame.

$$\hat{\mathbf{n}} = \frac{\hat{\mathbf{t}} \times (v'_1 - O'_i)}{|(\hat{\mathbf{t}} \times (v'_1 - O'_i))|} \tag{7}$$

Step 5: the local frame z-axis is formed from the unit vector of the cross product between $\hat{\mathbf{t}}$ and $\hat{\mathbf{n}}$.

$$\hat{\mathbf{b}} = \frac{(\hat{\mathbf{t}} \times \hat{\mathbf{n}})}{|(\hat{\mathbf{t}} \times \hat{\mathbf{n}})|} \tag{8}$$

2) Transformation Matrices: To translate coordinates from $\mathbb{R}^3$ onto the $\mathbb{R}^2$ plane, a transformation matrix can be determined, such that multiplying $\mathbb{R}^3$ coordinates with the matrix produces the new coordinates in $\mathbb{R}^2$.

Step 6: translation to the new x, y & z-axes is performed using the unit vectors, which are combined to produce the new Global $\rightarrow$ Local transformation matrix, as given by Equation 9.

$$\mathbf{G} = \begin{bmatrix} \hat{t}_x & \hat{b}_x & \hat{n}_x \\ \hat{t}_y & \hat{b}_y & \hat{n}_y \\ \hat{t}_z & \hat{b}_z & \hat{n}_z \end{bmatrix} \tag{9}$$

Step 7: let **P** denote the current position of a vehicle in $\mathbb{R}^3$ and **Ob** the position of an object O. Before translation, the position of O must be subtracted from **P**: **Ps = P - Ob**.

Step 8: **G** is now used to translate coordinates from the global to the local plane.

$$[Ps'] = [G]\,[Ps] \tag{10}$$

Step 9: the vehicle's position is converted back from $\mathbb{R}^2$ into $\mathbb{R}^3$ using the transpose of **G**.

$$[Ps] = [G^T]\,[Ps'] \tag{11}$$

Step 10: finally the object coordinates **Ob** are added to **Ps** to give its true position within $\mathbb{R}^3$.

E. Main Findings

The MATLAB software package was used to test the validity of the proposed approach, and compared it against a similar method employing a purely horizontal repulsive force surrounding each object. A scenario was utilised within which a pair of vehicles were given the task of surveying five objects (around opposite sides of their boundaries) in a 3D environment. To fully evaluate the method, the objects are such arranged that the vertical ascent of both vehicles is increased throughout their journey. It is assumed that each vehicle has omnidirectional movement with six degrees of freedom and a negligible turning radius. Vehicles operate at a constant velocity within a disturbance free environment, thus the only threats are either object or inter-vehicle collisions.

The scenario described above was performed first using horizontal repulsion for the rotational fields, then followed by the proposed technique involving 2D sub-planes, the results are shown below in Figs 4 & 5 respectively.

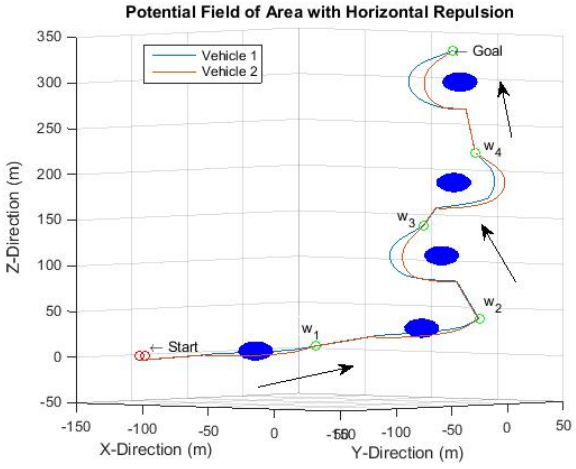

Fig. 4: The survey of five objects using horizontal rotational fields

Figs 4 and 5 show the effectiveness of the method and prove that a constant and definable distance can be maintained from an object surface regardless of approach direction, ideal for inspection missions. It was also established that journey time was reduced by 40% using the $\mathbb{R}^2$ planes (see [**?**] for full experimental results with numerical analysis).

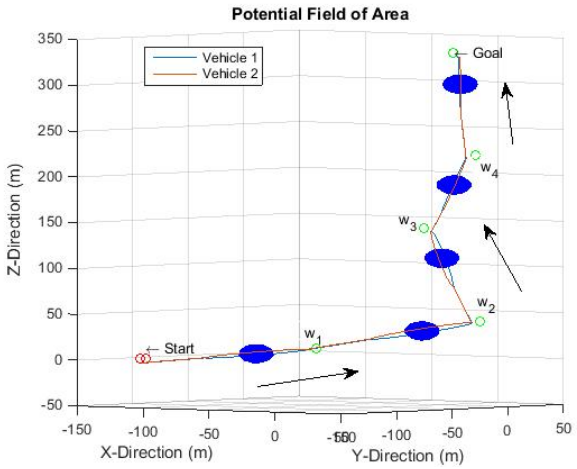

Fig. 5: The survey of five objects using 2D sub-planes

IV. Problem Statement with Proposed Methodology

A major problem with the survey of underwater structures involving more than one vehicle is ensuring vehicles are appropriately guided and positioned throughout the journey to provide a full inspection whilst minimising the path length. Appropriate inter-vehicle distances must be maintained, coupled with a pre-specified distance from all structural surfaces for collision prevention. In the case of an offshore oil rig platform for example, the inspection of each supporting column must by necessity cover the span of its entire depth below the surface. To achieve this, vehicles are guided to each column in turn using traditional APFs whilst opposing RPFs are used in order to guide vehicles in $\mathbb{R}^2$ sub-planes up and down each column using a concertina effect (with the distance-to-surface and number of loops determined by the user).

Using RPFs in this unconventional manner allows a pair of vehicles to cover an entire column surface using only this concertina or looping effect. The main advantage of rotational fields is the minimisation of the local minima problem, while the GNRON issue is eliminated by adjustable waypoints. Adjustable parameters allow for varying object sizes and inter-vehicle forces are such as to hold a fluid formation yet permit splitting for boundary inspection.

To provide a detailed description of the technique, an example will be used of a square, four-platform offshore oil rig platform. Initial parameters need to be set i.e. inter-vehicle distance, number of loops around each column and preferred distance-to-surface for inspection. A pair of vehicles (v_1 and v_2) will swim to the nearest edge (top or bottom) of the closest column before looping in a concertina effect around its entire length. Both vehicles then swim to the next closest column and the method is repeated until a full survey has been concluded.

Challenges: A number of new challenges are faced with a ground-based structure using a two-vehicle $\mathbb{R}^2$ sub-plane approach to ensure full survey capabilities while reducing path length and preventing collisions:

(A) Choosing the order in which legs are surveyed for path minimisation.
(B) Ensuring vehicle waypoints are positioned appropriately for movement to the next leg in turn.
(C) Allowing adjustable survey parameters e.g. how many times each leg is circled along its depth, distance from column surface etc.
(D) Creating a suitable survey plane within $\mathbb{R}^2$ to prevent collision with columns.

A number of steps are taken to tackle these challenges in turn as outlined below:

A. Column order for path minimisation

Reducing path length conserves energy and diminishes the potential for problems such as faults and collisions. As each column will be scanned in turn it is important to determine the order in which this is performed to ensure a structured approach. Vehicles can scan columns by moving upwards *or* downwards therefore it is logical to measure the distance to either the base or top of the structure depending on v_1's initial position to reduce its journey. At the start of each mission the depth of v_1 is measured (e.g. with an IMU or dedicated pressure sensor) and compared to the known height of the columns, then, depending on v_1's depth the distances are measured to either the top or base of all four columns. Using the vector from v_1 to the closest column, angles are subsequently measured along the x - y plane to the two columns equidistant from column one, in a similar manner to the technique shown in Section III-C. These are then compared in size to generate the smoothest path between the first and second column. The distance values are then arranged in size and stored in an array, along with their corresponding angles.

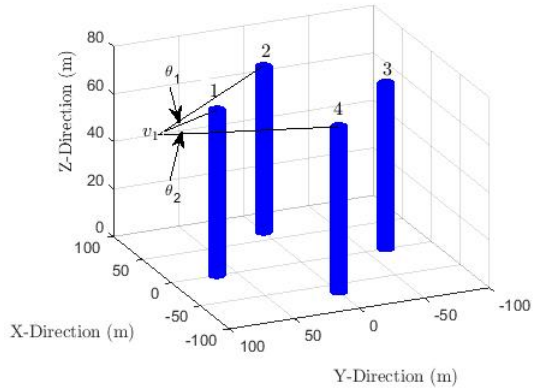

Fig. 6: Initial distance and angle calculations

It can be seen from Fig 6 that as v_1's starting depth lies closer to the top of the columns than the base, the tops are used for initial distance measurements. Columns have been given arbitrary numbers in this instance and as column 1 lies closest to v_1, it is taken as the first to be surveyed. To further reduce path length, angles are measured from v_1 to columns 2 & 4 (both closest to, and equidistant from column 1) and

compared to the angle between v_1 and column 1 to determine which column should be surveyed next. It can be seen that as $\theta_1 < \theta_2$ the closest correlation is between columns 1 & 2 so 2 is chosen as the second one to survey. The order in which the third and fourth column are chosen will be determined in the next part.

B. Waypoints placement for navigation

A structured framework is required to guide both vehicles towards a column and to leave them at a suitable position for travel towards the next one, in order to minimise the overall journey. Utilising a technique similar to that in [29] it is reasoned that two waypoints can be placed at the apex and base of every column (four waypoints per column at a user definable distance d_{ow} from the column core on the $x-y$ plane) with their alignment such as to leave a vehicle as close as possible to the next column where appropriate. To illustrate this, placing two waypoints at the top of column 1 in alignment with column 2 involves the use of a virtual line which passes through the apex of both columns. Two waypoints are then placed upon this line at either side of column 1 - one nearside to column 2 and the other farside (these points are equidistant from column 1 at a user determinable length horizontally from its core) using the following equations.

$$x_n = \frac{a_2 x_1}{a_1 + a_2} + \frac{a_1 x_2}{a_1 + a_2} \tag{12}$$

$$y_n = \frac{a_2 y_1}{a_1 + a_2} + \frac{a_1 y_2}{a_1 + a_2} \tag{13}$$

$$x_f = \frac{x_2(a_1 + 2a_2) - a_2 x_1}{a_1 + a_2} \tag{14}$$

$$y_f = \frac{y_2(a_1 + 2a_2) - a_2 y_1}{a_1 + a_2} \tag{15}$$

Where a_1 is the horizontal distance from column two's core to the nearside waypoint, a_2 is the horizontal distance from the nearside waypoint to column one's core, (x_1,y_1) are the coordinates of the top of column two's core on the $x-y$ plane, (x_2,y_2) are the coordinates of the top of column one's core on the $x-y$ plane, (x_n,y_n) and (x_f,y_f) are the coordinates of the near and farside waypoints respectively.

This process is then repeated for the base of column 1 before applying the same overall method to column 2. As the first two optimum columns have been chosen based on vehicle start positions, a scan can then be performed from the last waypoint on columns two and three to determine the next closest leg using the caveat that the scan now falls beyond 1.2*d_{ow} to ensure no return to a previous column.

Fig 7 displays the validity of this approach where fifteen intermediary waypoints are numbered (two each on the top and bottom of every column), providing an avenue for vehicles to be manoeuvred efficiently around the entire structure. It is shown for example that w_1-w_4 are placed such as to provide guidance first towards the top of column one (w_1 - the closest point to v_1)

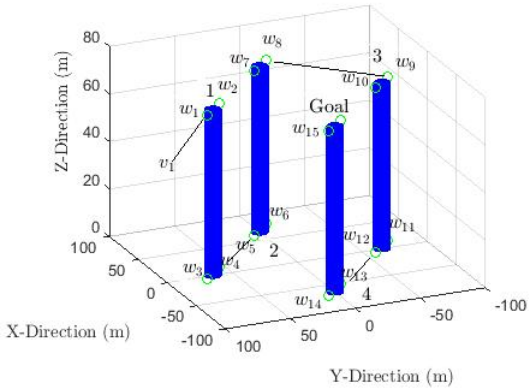

Fig. 7: Initial waypoint placement

and also place vehicles (following column survey) at a location where they can then swim directly towards column two (w_4 - w_5). Lines are placed in the figure where the intermediary journeys take place between actual column surveys.

C. Adjustable survey parameters

Fig 7 showed four waypoints per column and these can be utilised to create both near and far side virtual columns on which to place a number of zigzagging waypoints. The number of waypoints is user-determinable depending on the detail requirements of the survey. By way of illustration, in Fig 8 five slanting loops have been determined (every column will have a horizontal loop at its top and base to inspect the join at both platform and ground), therefore virtual lines are formed on the nearside and far side from $w_1 \rightarrow w_7$ and $w_2 \rightarrow w_8$ respectively, these are then used to place w_3-w_6 in a staggered effect as start and end points for the five $\mathbb{R}^2$ sub-planes. Other adjustable parameters include inter-vehicle formation distance, range of repulsion from object surface, distance of waypoints from surface etc.

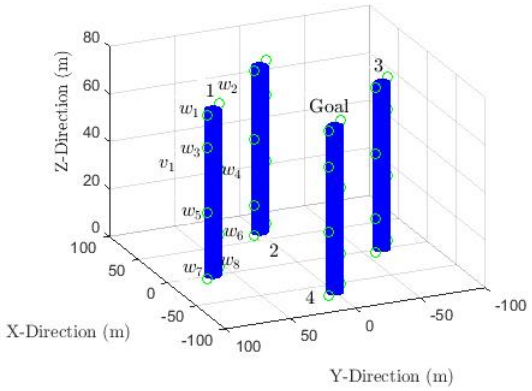

Fig. 8: Waypoints placement

D. Formation of suitable $\mathbb{R}^2$ sub-planes

One of the advantages of the fluid formation technique is that vehicle pairs are devoid of angular constraints and are free to

swim at any position relative to the other with their separation being the only determinable factor. In Section III-D an $\mathbb{R}^2$ sub-plane was generated when a pair of vehicles enters the repulsive sphere surrounding an object with the plane lying on v_1, v_2 and the object's centroid. As vehicles are only constrained by their separation distance the plane can be formed at any angle relative to an earth-fixed frame yet still allow boundary coverage for some objects in three dimensions underwater. This is unsuitable for ground-based vertical columns. For a start, v_1 and v_2 are free to approach a column at any angle with respect to each other so may arrive vertically, horizontally or at any intermediate angle. Secondly, to allow variable levels of survey by increasing the number of loops up and down the column it is clear that the object centroid cannot lie on the plane, except in the case of a single loop from top to bottom.

In order to rectify these issues and allow the number of loops to be determined by the user, the midpoint m_w is chosen between waypoints on the zigzagging formation for each sub-plane - this is in place of the object centroid from Section III-D. Then, as v_1 & v_2 enter the column's repulsive range, their midpoint m_v is taken as the second point to lie on the plane. A small extrapolation from m_v in an $x-y$ direction is then used as the third and final point to enable provision of a controllable boundary plane for survey.

Both the loop count and repulsion range can be adjusted to allow for a general or detailed survey approach for differing vehicle types, camera calibration etc.

V. Results

To evaluate the proposed concertina method's efficacy and survey ability, two different scenarios have been simulated using the MATLAB software suite.

A. Scenario 1

A scenario involving two vehicles and a four-column platform was employed with a seven loop survey count - note as the apex and base of every column is fixed to a flat surface (i.e. the offshore platform and sea bed), both extremities on each column are surveyed using a horizontal loop to ensure a full inspection. Start coordinates for v_1 & v_2 are (-20,60,75) and (-15,65,85) respectively, columns have height h=70 m, radius r_l=6 m and centre base coordinates (65,0,0),(0,-65,0),(-65,0,0) and (0,65,0). Waypoint distance is set at d_{ow}=12 m from each column's core with repulsion range set at r_{o_i}=4 m from their surface. Inter-vehicle formation distance s_v=1 m and waypoint COA radius w_r=1.5 m, with force scale factors shown in Table I.

TABLE I: Scale factor quantities for potential field equations

Force Scale Factors for Potential Fields			
Attractive Goal or Waypoint k_a	Object Repulsion k_o	Inter-vehicle Attraction k_v	Inter-vehicle Repulsion k_r
1	1×10^{8}	1×10^{-5}	3

In Figs 9 and 10 it can be seen that both vehicles are successfully guided towards the top of the closest column,

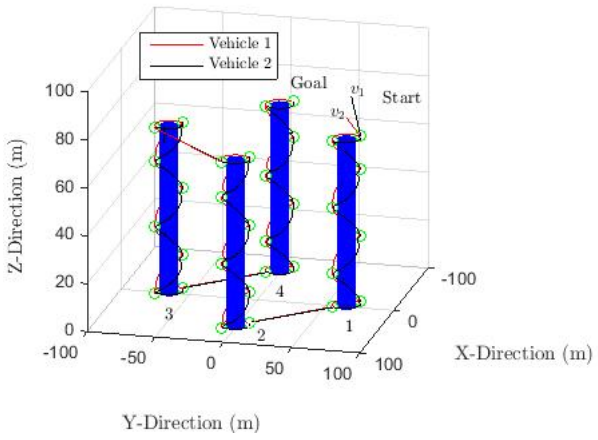

Fig. 9: Inspection of oil rig using five loop concertina effect - 3D view

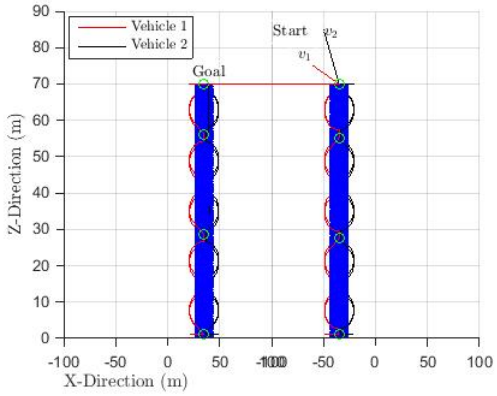

Fig. 10: Inspection of oil rig using five loop concertina effect - side on view

where they then loop downwards, covering the entire depth of the column. From the base of column 1 both v_1 and v_2 swim directly to the base of column 2 before looping up towards its apex and then moving on to column 3. All columns are successfully inspected before vehicles arrived at the final goal point.

In Fig 11 the elevation of both v_1 and v_2 is plotted throughout the entire journey from their initial start positions until all four columns have been surveyed and the final waypoint reached. Fig 12 then displays the distance between both vehicles for the entire trajectory, showing a uniform increase/decrease seven times during the survey of each of the four columns.

B. Scenario 2

To demonstrate the suitability for different sized structures and varying parameters a further scenario was simulated featuring a smaller structure. This time the columns had height h=40 m, radius r_l=6 m and centre base coordinates (45,0,0),(0,-45,0),(-45,0,0) and (0,45,0). A tighter inspection was performed with thirteen loops per column and repulsion range was set

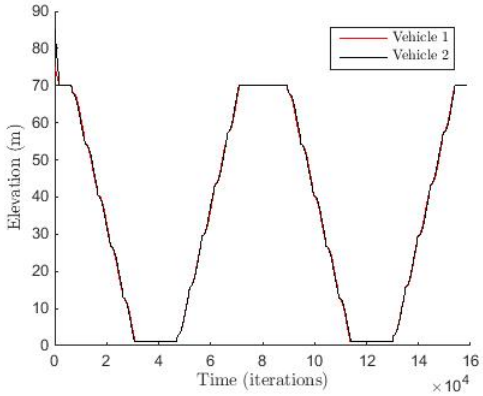

Fig. 11: Vehicle elevation (m)

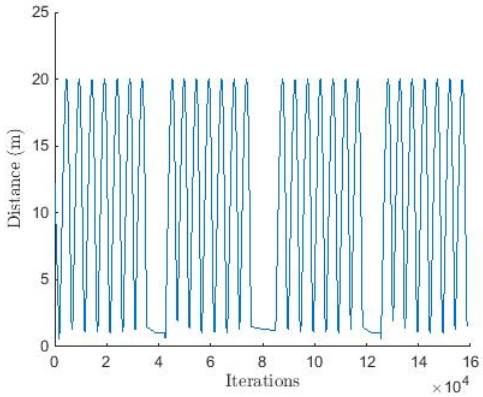

Fig. 12: Inter-vehicle distance (m)

at r_{o_i}=2 m from the columns' surface. Vehicles were initially placed closer to the sea floor ((-20,70,10) and (-10,73,12) for v_1 and v_2 respectively) to verify whether they would start at the base of the closest column, and waypoint distance was halved to d_{ow}=6 m from the columns' core. Inter-vehicle distance, waypoint COA and force scale factors were as before.

In Fig 13 it can be seen that both vehicles swim towards the bottom of the closest column, where they then loop upwards in a tighter form than previously, covering its entire height. From the top of this column they then move directly to the top of column 2 and repeat the survey process until the whole structure has been inspected.

VI. Analysis and Discussion

A proper analysis of the results will best be served in light of the initial challenges posited in Section IV i.e.

a) Choosing the order in which legs are surveyed for path minimisation.
b) Ensuring vehicle waypoints are positioned appropriately for movement to the next leg in turn.
c) Allowing adjustable survey parameters e.g. how many times each leg is circled along its depth, distance from column surface etc.

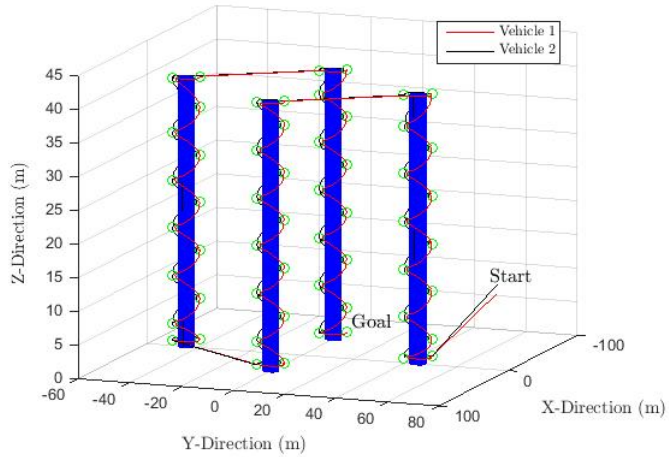

Fig. 13: Smaller platform with tighter inspection - 3D view

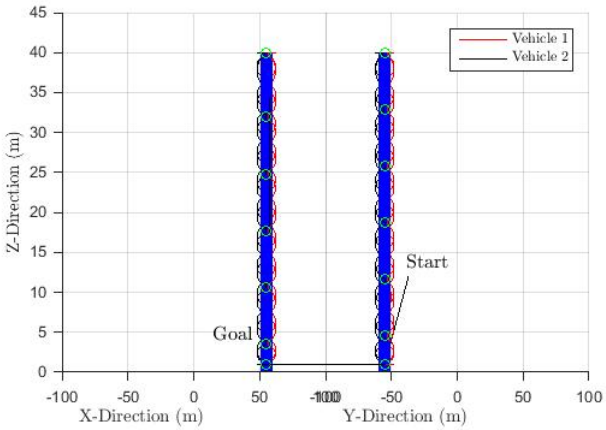

Fig. 14: Smaller platform with tighter inspection - side on view

d) Creating a suitable survey plane within $\mathbb{R}^2$ to prevent collision with columns.

a) Figs 9 and 10 show that both vehicles swim towards the closest edge of the nearest column from their start positions and it can also be observed that the second column surveyed is the closest in line with both the start position of v_1 and the first column chosen, showing the effectiveness of the method proposed in Section IV-A. The ability to achieve a complete survey by the shortest path possible regardless of vehicle start position (different start positions are shown in Scenario 2 - Fig 13) maximises power saving and helps to reduce the threat of collision.

b) As Figs 9 and 10 show, waypoints have been strategically placed allowing the same level of inspection for all four individual columns. Taking columns 1 and 2 as examples, although each column contains the same number and arrangement of waypoints, these are not a set pattern arbitrarily placed around each column but are positioned such that the final waypoint on column one corresponds to the initial one on column two to minimise path length and maximise ease of approach (please

refer to Fig 11 for the close correlation of both vehicles' elevation throughout the entire survey mission). This method of arrangement occurs irrespective of the vehicles' start positions and orientation to the overall structure (see Figs 13 & 14 for a scenario with different start positions).

c) Two different scenarios were deliberately simulated using varying parameters to investigate the technique's effectiveness. Vehicle start positions along with loop count and repulsion range from the surface of each column were varied and in both instances a collision-free journey with minimum trajectory was obtained. To verify the parameters' effectiveness, take for example the user-defined distances for vehicle separation sv=1 m, column radius r_l=6 m and repulsion range r_{o_i}=4 m in Scenario 1. Given these values, it should be expected that as vehicles loop around each column their separation distance would vary from 1 m to 20 m in a concertina effect. This is verified and observed in Fig 12 with the closest inter-vehicle distance throughout the entire journey recorded at 0.58 m.

d) While the work presented in [**?**] provided ideal sub-planes for inspection of 3D objects, due to the fluid nature of the vehicle formation it is unsuitable for ground-fixed structures. However, using both m_w and m_v to generate the $\mathbb{R}^2$ sub-planes has allowed substantial controllability and the smooth looping trajectories which can be seen in Fig 9. In Scenario 1, Fig 10 displays a side view (two columns directly obscured by columns in front) emphasising the similarity of the sub-planes which look identical from this angle (see also Fig 14 in Scenario 2). Further confirmation of the fixed looping trajectories can be found in Fig 12 where the inter-vehicle separation increases and decreases uniformly during survey with the same maximum value recorded for every loop and no collisions; Fig 11 shows the elevation of v_1 & v_2 throughout the journey and highlights the high level of cooperation between both vehicles as they survey the opposite sides of every column.

VII. Conclusion

In this paper a unique method has been shown for the inspection of underwater structures using autonomous vehicles in three dimensions. Vehicles were guided in a flexible formation, free of angular constraints (reducing computational load) towards the supporting columns of an offshore oil platform using traditional APFs, whilst opposing RPFs were utilised on 2D sub-planes for column inspection using a concertina effect. Vehicles are guided such as to perform a complete survey with minimum path length. Simulation work was successfully performed on two different scenarios without local minima issues or the GNRON problem common in potential field work.

Acknowledgment

The first author would like to acknowledge the Department of Employment and Learning, Northern Ireland for funding the research.

References

[1] SMD. (2016) Product home page. [Online]. Available: https://smd.co.uk/products/trenchers-self-propelled/qtrencher-2800.htm

[2] O. ROV. (2016) Product home page. [Online]. Available: http://www.openrov.com/

[3] S. Pai and R. Hine, "Successful execution of remotely piloted autonomous marine vehicles to conduct METOC and Turbidity surveys," in *2014 IEEE/OES Autonomous Underwater Vehicles (AUV)*. Oxford, England: IEEE, October 2014, pp. 1–3.

[4] D. Bingham, T. Drake, U. Kingdom, and A. Hill, "The Application of Autonomous Underwater Vehicle (AUV) Technology in the Oil Industry Vision and Experiences," *TS4.4 Hydrographic Surveying II*, vol. XXII, pp. 1–13, 2002.

[5] T. Salgado-Jimenez, J. L. Gonzalez-Lopez, J. C. Pedraza-Ortega, L. G. Garcia-Valdovinos, L. F. Martinez-Soto, and P. A. Resendiz-Gonzalez, "Design of ROVs for the Mexican power and oil industries." Montreal, Canada: IEEE, October 2010, pp. 1–8.

[6] B. Fletcher, "UUV master plan: a vision for navy UUV development," in *OCEANS 2000 MTS/IEEE Conference and Exhibition. Conference Proceedings (Cat. No.00CH37158)*, vol. 1. Providence, RI: IEEE, September 2000, pp. 65–71.

[7] M. Federis. (2016, July) Growing popularity of underwater drones raises similar concerns as aerial counterparts. [Online]. Available: http://www.capradio.org/articles/2016/07/01/growing-popularity-of-underwater-drones-raises-new-questions/

[8] T. O. P. Team. (2016, October) Gulf oil spill. [Online]. Available: http://ocean.si.edu/gulf-oil-spill

[9] S. Evans. (2016, January) Mh370 search drone disappears after slamming into underwater mud volcano during missing plane hunt. [Online]. Available: http://www.mirror.co.uk/news/uk-news/mh370-search-drone-disappears-after-7239581

[10] Statista.com, "Number of offshore rigs worldwide as of 2015, by region," 2015, (Date last accessed 30-01-2017). [Online]. Available: https://www.statista.com/statistics/279100/number-of-offshore-rigs-worldwide-by-region/

[11] T. C. Estate, "Offshore wind electricity map," 2017, (Date last accessed 30-01-2017). [Online]. Available: https://www.thecrownestate.co.uk/energy-minerals-and-infrastructure/offshore-wind-energy/offshore-wind-electricity-map/

[12] L. G. Association, "How much do wind turbines cost and where can i get funding?" 2015, (Date last accessed 30-01-2017). [Online]. Available: http://www.local.gov.uk/home/-/journal_content/56/10180/3510194/ARTICLE

[13] T. S. Institute, "A fresh start on a floating city could be just a few years away," 2014, (Date last accessed 30-01-2017). [Online]. Available: https://www.seasteading.org/floating-city-project/

[14] A. Sehgal, D. Cernea, and A. Birk, "Modeling underwater acoustic communications for multi-robot missions in a robotics simulator," in *Oceans'10 IEEE Sydney*. Australia: IEEE, May 2010, pp. 1–6.

[15] J. Mccolgan and E. W. Mcgookin, "Coordination of a School of Robotic Fish using Nearest Neighbour Principles," in *OCEANS 2014 - TAIPEI*. Taipei: IEEE, April 2014, pp. 1–8.

[16] D. Edwards, T. Bean, D. Odell, and M. Anderson, "A Leader-Follower Algorithm for Multiple AUV Formations," *2004 IEEE/OES Autonomous Underwater Vehicles (IEEE Cat. No.04CH37578)*, pp. 40–46, June 2004.

[17] C. B. Low, "A Dynamic Virtual Structure Formation Control for Fixed-Wing UAVs," in *IEEE International Conference on Control and Automation, ICCA*, Santiago, Chile, December 2011, pp. 627–632.

[18] O. Khatib, "Real-Time Obstacle Avoidance for Manipulators and Mobile Robots," in *Robotics and Automation. Proceedings. 1985 IEEE International Conference on (Volume:2)*, March 1985, pp. 500–505.

[19] J. M. Esposito, "Decentralized cooperative manipulation with a swarm of mobile robots," *2009 IEEE/RSJ International Conference on Intelligent Robots and Systems, IROS 2009*, pp. 5333–5338, June - July 2009.

[20] X. Chen and J. Zhang, "The three-dimension path planning of uav based on improved artificial potential field in dynamic environment," in *Intelligent Human-Machine Systems and Cybernetics (IHMSC), 2013 5th International Conference on*, vol. 2. IEEE, 2013, pp. 144–147.

[21] B. K. Sahu, B. Subudhi, and B. K. Dash, "Flocking control of multiple autonomous underwater vehicles," in *2012 Annual IEEE India Conference (INDICON)*. IEEE, 2012, pp. 257–262.

[22] Q. Zhu, Y. Yan, and Z. Xing, "Robot Path Planning Based on Artificial Potential Field Approach with Simulated Annealing," in *Sixth International Conference on Intelligent Systems Design and Applications*, vol. 2, Jinan, October 2006, pp. 622–627.

[23] S. Molotchnikoff and J. Rouat, *Visual Cortex - Current Status and Perspectives*. The Authors, 2012.

[24] J. Sfeir, M. Saad, and H. Saliah-Hassane, "An improved artificial potential field approach to real-time mobile robot path planning in an unknown environment," in *Robotic and Sensors Environments (ROSE), 2011 IEEE International Symposium on*. IEEE, 2011, pp. 208–213.

[25] A. D. Dang and J. Horn, "Path Planning for a Formation of Autonomous Robots in an Unknown Environment Using Artificial Force Fields," *Proceedings of the 18th International Conference on System Theory, Control and Computing, Sinaia, Romania, October 17-19, 2014*, pp. 773–777, October 2014.

[26] H. Rezaee, S. Member, and F. Abdollahi, "Mobile Robots Cooperative Control and Obstacle Avoidance Using Potential Field," *Proceedings of the 2011 IEEE/ASME International Conference on Advanced Mechatronics (AIM2011)*, July 2011.

[27] H. Rezaee and F. Abdollahi, "Adaptive artificial potential field approach for obstacle avoidance of unmanned aircrafts," in *2012 IEEE/ASME International Conference on Advanced Intelligent Mechatronics (AIM)*. IEEE, 2012, pp. 1–6.

[28] D. McIntyre, W. Naeem, and S. S. A. Ali, "Underwater surveying and mapping using rotational potential fields for multiple autonomous vehicles," in *6th IEEE International Conference on Underwater System Technology: Theory & Applications (USYS16), Pulau Pinang, Malaysia*. IEEE, 2016, pp. 1–6.

[29] D. McIntyre, W. Naeem, and C. Zhang, "Cooperative mapping and exploration using counter-rotational potential fields," in *Signals and Systems Conference (ISSC), 2016 27th Irish*. IEEE, 2016, pp. 1–7.